Taylor & Francis
Taylor & Francis Group

Check for updates

High-order overset grid method for detecting particle impaction on a cylinder in a cross flow

Jørgen R. Aarnes [a], Nils E. L. Haugen[a,b] and Helge I. Andersson[a]

[a]Department of Energy and Process Engineering, Norwegian University of Science and Technology, Trondheim, Norway; [b]SINTEF Energy Research, Trondheim, Norway

ABSTRACT

An overset grid method was developed to investigate the interaction between a particle-laden flow and a circular cylinder. The method is implemented in the Pencil Code, a high-order finite-difference code for compressible flow simulation. High-order summation-by-parts operators were used at the cylinder boundary, and both bi-linear Lagrangian and bi-quadratic spline interpolation were used to communicate between the Cartesian background grid and the body-conformal cylindrical grid. The performance of the overset grid method was assessed to benchmark cases of steady and unsteady flows past a cylinder. Results show high-order accuracy and good agreement to the literature. Particle-laden flow simulations were performed, with inertial point particles impacting on a cylinder. The simulations reproduced results from the literature at a significantly reduced cost. Further, an investigation into blockage effects on particle impaction revealing that the previously published DNS data is less accurate than assumed for particles with very small Stokes numbers.

1. Introduction

A common flow problem in numerical simulations is flow past a bluff body. Obstructions in the flow include (but are not limited to) spheres, flat plates, circular, rectangular or elliptical cylinders, triangles, spheroids and complex geometries made out of a combination of these shapes. Particle-laden flows interacting with such obstacles are important for a range of applications. Whether the goal is to maximise the particle extraction from the flow, as for filter applications, or to minimise particle attachment on the object to avoid an insulating layer, as for biomass boilers, understanding the mechanics of inertial particles helps improve design, and hence, the efficiency of said applications. Accurate prediction of particle behaviour in the vicinity of bluff bodies requires highly accurate boundary layer representation within numerical simulations. Finding the numerical method best suited to this task is not trivial, and can have a huge impact on both the efficiency and accuracy of simulations.

1.1. Representing solid objects in the flow

For generic shapes (cylinders, spheres, plates, etc.) body-fitted structured meshes are commonly used to accurately resolve the solid boundary. These methods use grids that conform to the solid (or solids) immersed in the flow and to other physical boundaries of the domain (inlet/outlet, walls, etc.). Depending on the domain's geometry, this may require some deformation of the grid to conform to the boundaries, in addition to the mapping of the flow domain onto a simple computational domain. The result may lead to unnecessary local variations in the grid and rather time consuming grid generation (Versteeg and Malalasekera 2007). Alternatively, unstructured meshes can be applied to resolve the solid boundaries in the flow. Unstructured meshes provide the highest flexibility in adapting a mesh to the flow problem, and are a good alternative for complex geometries when finite-volume or finite-element formulations of the governing equations are used (Mavriplis 1997). Among the disadvantages of such grids are much

---

CONTACT Jørgen R. Aarnes ✉ jorgen.r.aarnes@ntnu.no

larger storage requirements (Tannehill, Anderson, and Pletcher 1997) and the need for intricate mesh generation techniques (Owen 1998).

An alternative to body-fitted grids are non-conforming (typically Cartesian) meshes, where a solid in the flow is represented by a change in the fluid equations in the vicinity of the solid boundary. One such method, which has gained vast popularity over the last decades, is the immersed boundary method (IBM). This method (or rather, this class of methods) was originally developed to model flow around heart valves (Peskin 1972) by allowing for the representation of bluff bodies in the flow without using a body-conformal grid. A simple Cartesian grid can be used, with the boundary conditions (the sharp interface) of the bluff body incorporated into the solver by a modification of the equations in the vicinity of the boundary (see review article by Mittal and Iaccarino (2005) and references therein for details). This makes IBMs very flexible for representing bluff bodies, and particularly well-suited to complex geometries, where the use of body-fitted structured meshes is limited. A caveat to the IBM is the difficulty in achieving high-order accuracy near boundaries that do not conform to the grid. For complex geometries this may be regarded as a necessary loss in order to be able to represent the boundary. For flow past simple geometries other methods may be more suitable, especially when the accuracy in the vicinity of the surface is of major concern.

Roughly 10 years after the initial development of the IBM, a method of multiple grids *overset* on top of one another was proposed to represent solids in a flow (see Steger, Dougherty, and Benek 1983; Benek, Buningt, and Steger 1985; Steger and Benek 1987). Overset grids, or Chimera methods, employ body-conformal grids at the bluff bodies, but the body-conformal grids do not extend to the domain boundaries. Instead, a non-body-conformal background grid (typically uniform Cartesian) is used, and updated flow information within overlapping grid regions is communicated between grids at every time step. In this way, the flow simulation is split into multiple sub-simulations, one for each grid, and the boundaries of one grid are updated with information from the other grids. The background grid is used to compute the general flow field outside the smaller body-fitted grids, and the communication between grids is achieved through interpolation.

Overset grid methods have the advantage of being highly accurate at the solid–fluid interface. This is due to the use of body-fitted grids in these regions, and the flexibility in grid stretching made possible when several grids are used. At the same time, no grid deformation is necessary to conform to domain boundaries, due to the use of an appropriate non-conformal background grid. If the domain is circular, a cylindrical grid can be used as a background grid, if the domain is rectangular, a Cartesian grid, etc.

The communication between the grids is the limiting factor in terms of the accuracy of overset grid methods. In general, the interpolation of flow variables is detrimental to mass conservation (although conservative, mass correcting overset grid methods do exist for finite-volume codes, see e.g. Pärt-Enander and Sjögreen 1994 and Zang and Street 1995). Using high-order interpolation between grids has proved beneficial in regards to the overall accuracy and stability of the overset grid method for both finite-difference and finite-volume implementations (Sherer and Scott 2005; Chicheportiche and Gloerfelt 2012; Völkner, Brunswig, and Rung 2017). While advantageous in terms of accuracy, high-order interpolation techniques have the disadvantage of increase in complexity, inter-processor communication and floating-point operations, when compared to low-order interpolation schemes. Furthermore, straightforward extension to high-order interpolation, typically from second-order to fourth-order Lagrangian interpolation, does not guarantee a better solution. Possible overshoots in the interpolation polynomials may have a devastating impact on the interpolation accuracy. The applied interpolation scheme should therefore be evaluated for the specific flow problem at hand. For overset grid implementations, several interpolation schemes are available. In this study two such schemes are compared: bi-linear Lagrangian interpolation and bi-quadratic spline interpolation. Together with high-order low-pass filtering, the resulting computations were both stable and accurate. This topic is further discussed in Section 2.

If several body-fitted grids overlap, the overset grid computations become increasingly difficult, particularly in regards to the communication between the different grids. For the purposes of this paper, the discussion is limited to a single body-fitted grid on top of a Cartesian background grid (for a more general

discussion on overset grids, see Meakin 1995 or Chesshire and Henshaw 1990). A recent development of multiple-grid systems using overset grids can be found in the work by Vreman (2016) and Vreman and Kuerten (2018), where DNS simulations of spherical fully resolved particles are achieved by an individual spherical grid attached to each particle. Applications to DNS of particle-laden flows are indeed the purpose of our method as well, but due to the high count of small particles required for our deposition simulations, fully resolved particles are not an option at present. Hence, we restrict the use of overset grids to the solid surface onto which the particles are impinging.

1.2. Particle impaction

When considering particle deposition on a surface, two mechanisms are required for a particle to deposit. The particle must first impact the surface, that is, it must physically contact the surface, and then it must adhere to the surface. Only the first of these two mechanisms will be the focus of this study. Hence, all particles that come into contact with the bluff body are considered to have been absorbed by it. Further, only inertial impaction is considered. Any other particle impaction mechanisms including Brownian motion, thermophoresis and turbulent diffusion are omitted. Note that this is not an acceptable omission in non-isothermal flows, where the effects of temperature will be large on small particles (see Beckmann et al. 2016; García Pérez, Vakkilainen, and Hyppänen 2016).

The impaction efficiency $\eta = N_{imp}/N_{ins}$ is a measure of the cylindrical object's ability to capture the particles that are initially incident on the cylinder. The number of impacting particles is given by N_{imp}, while N_{ins} is the count of particles with a centre of mass that is initially moving in the direction of the solid object. Note that following this convention may lead to $\eta > 1$, even if no forces act on the particles, since a particle may follow a path close enough to be intercepted by the object, due to its finite size, even though the centre of mass does not hit the object.

A fluid flow will be deflected by the object, and particles in the flow will experience a drag force. This force will accelerate the particles along the fluid trajectory, leading particles away from the bluff body. The particle Stokes number, $St = \tau_p/\tau_f$, where τ_p and τ_f are particle and fluid time scales, respectively (details in Section 4), can be considered a measure of particle inertia. Hence,

particles with a small Stokes number follow the flow to a larger extent than particles with a large Stokes number. By using potential flow theory to compute the flow past a circular cylinder, Israel and Rosner (1982) determined a relation for the impaction efficiency as a function of the Stokes number. The predictions by Israel and Rosner (1982) are inaccurate in predicting particle impactions for flows where the viscous boundary layer of the cylinder plays a significant role. This is because potential flow theory assumes inviscid flow. In particular, this theory is insufficient at predicting impactions for particles with small Stokes numbers, and for moderate Reynolds number flows. Here, the Reynolds number is defined as $Re = U_0 D/\nu$, where U_0 is the mean flow velocity, D is the diameter of a cylinder (the bluff body in the flow) and ν is the kinematic viscosity of the fluid.

Haugen and Kragset (2010) performed simulations using the Pencil Code to compute inertial particle impaction on a cylinder in a crossflow for different Stokes and Reynolds numbers. Later, similar studies have been performed with multiple cylinders (Haugen et al. 2013) and with turbulent free-stream flow (Aarnes, Haugen, and Andersson 2019). Although the impaction efficiencies obtained by Haugen and Kragset (2010) have been used as benchmarking results, the mentioned studies were limited to moderate Reynolds numbers or two-dimensional flows. Part of the reason for this limitation is the use of an immersed boundary method that requires a very fine grid to achieve the necessary accuracy.

1.3. Present contribution

The purpose of this paper is to introduce an overset grid method applicable to compressible particle-laden flows past a circular cylinder, and to assess its performance in benchmarking cases and a true particle-laden flow simulation. The method has been implemented in the open source compressible flow solver known as the Pencil Code (Brandenburg and Dobler 2002; The Pencil Code 2018), with the aim to improve the accuracy in the vicinity of the cylinder and to reduce the computational cost of particle-laden flow simulations.

The structure of the paper is as follows: In Section 2 the equations governing the flow and the bluff body representation are described. An assessment of the accuracy of the method for steady and unsteady flow

past a cylinder is given in Section 3. In Section 4 the capabilities of the overset grid method are demonstrated by simulating particle-laden flows interacting with a bluff body at a moderate Reynolds number. The computational costs and the accuracy of the results are compared with those of Haugen and Kragset (2010), before concluding remarks are given in Section 5.

2. Methodology

2.1. Governing equations

The governing equations of the flow are the continuity equation:

$$\frac{\mathrm{D}\rho}{\mathrm{D}t} = -\rho \nabla \cdot \boldsymbol{u}, \tag{1}$$

and the momentum equation:

$$\rho \frac{\mathrm{D}\boldsymbol{u}}{\mathrm{D}t} = -\nabla p + \nabla \cdot (2\mu \boldsymbol{S}), \tag{2}$$

where ρ, t, $\boldsymbol{u}$ and p are the density, time, velocity vector and pressure, respectively, and $\mu = \rho\nu$ is the dynamic viscosity. The compressible strain rate tensor $\boldsymbol{S}$ is given by:

$$\boldsymbol{S} = \frac{1}{2}\left(\nabla \boldsymbol{u} + (\nabla \boldsymbol{u})^{\mathrm{T}}\right) - \boldsymbol{I}\left(\frac{1}{3}\nabla \cdot \boldsymbol{u}\right), \tag{3}$$

where $\boldsymbol{I}$ is the identity matrix. The pressure is computed using the isothermal ideal gas law, $p = c_s^2 \rho$, where c_s is the speed of sound. The flow is isothermal and weakly compressible, with a Mach number of ~ 0.1 for all simulations. With a constant speed of sound (for the isothermal case) and a constant kinematic viscosity, the momentum equation to be solved on the overset grids is:

$$\frac{\mathrm{D}\boldsymbol{u}}{\mathrm{D}t} = -c_s^2 \nabla (\ln \rho) + \nu \left(\nabla^2 \boldsymbol{u} \right.$$
$$\left. + \frac{1}{3}\nabla (\nabla \cdot \boldsymbol{u}) + 2\boldsymbol{S} \cdot \nabla (\ln \rho) \right). \tag{4}$$

The governing Equations were discretised with sixth-order finite-differences in space and a third-order memory efficient Runge–Kutta scheme in time (Williamson 1980). The flow was simulated on a rectangular domain with an inlet at the bottom and flow in the vertical direction. The circular cylinder was situated in the centre of the domain, with the following boundary conditions: no-slip and impermeability for velocity, and zero gradient in the radial direction

for the density. The latter condition was derived from the ideal gas law and the boundary layer approximation ($\partial p / \partial n = 0$, where n is the wall normal direction) for an isothermal flow. Note that this is a first-order approximation, and the physical value of the wall-normal component of the pressure gradient on the wall will be nonzero. However, as the density fluctuations are very small near the solid surface, in particular when compared to the velocity fluctuations, this is not expected to have a significant impact on the overall accuracy.

Navier–Stokes characteristic boundary conditions were used both at the inlet and at the outlet of the flow domain. This boundary condition is a formulation that makes use of one-dimensional characteristic wave relations to allow acoustic waves to pass through the boundaries (Poinsot and Lele 1992; Yoo et al. 2005). The remaining domain boundaries were periodic.

2.2. Overset grids

To resolve the flow domain using an overset grid method, a cylindrical coordinate grid was body-fitted to the cylinder, and a uniform Cartesian grid was used as the background grid (see Figure 1(a)). The cylindrical grid was stretched in the radial direction. In the region where fluid data is communicated between grids, it is beneficial that the grids have similar spacing. The grid stretching enables similar grid spacing in the interpolation region and a much finer grid near the cylinder surface.

The compressibility of the flow leads to a strict stability limit for the Runge–Kutta method, imposing a very small time step in the simulations. Because the overset grid method is effectively solving two different flow problems, coupled only by the communication between the grids, there is flexibility in the choice of time step. Choosing a time step on the background grid that is small enough to guarantee stability for the Cartesian grid spacing, and choosing a smaller time step on the cylindrical grid reduces the overall computational cost significantly. The cylindrical grid time step must be a multiple of the background grid time step to ensure that the computations on each grid are synchronised. An implicit solver may be beneficial, if the grid spacing near the cylinder is several orders of magnitude smaller than that of the background grid, but that issue is beyond the scope of this study.
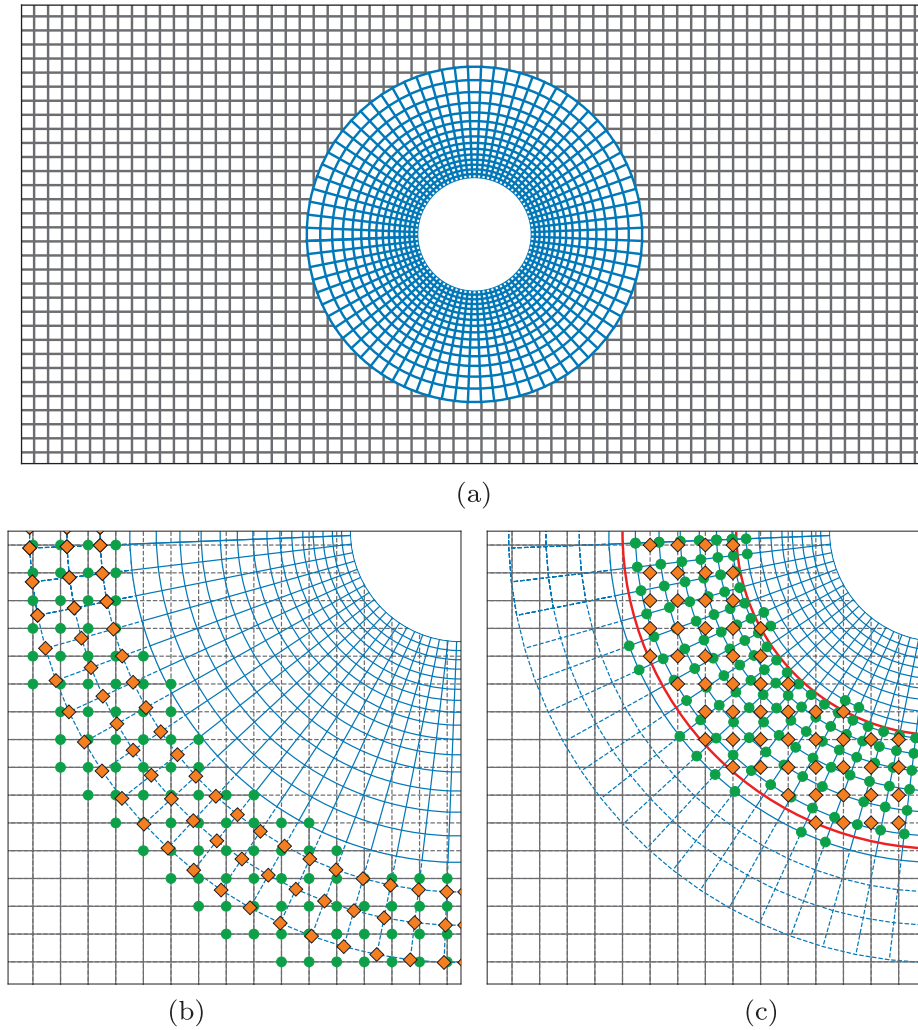
Figure 1. Overset grid method: (a) Cylinder grid on top of background grid (fringe-points of cylinder grid and background grid points within cylinder grid radius not shown). (b) Communication between grids, interpolation from Cartesian donor-points to cylindrical fringe-points. (c) Communication between grids, interpolation from cylindrical donor-points to Cartesian fringe-points. Four donor-points (●) surround each fringe-point (◇) in bi-linear interpolation. Dashed grid lines used to illustrate where the flow variables are not computed by finite-differences (fringe-points and hole-points).

The communication between the grids in the overset grid simulation was completed in two stages for each time step of the background grid. At each stage of the communication, the required flow properties were interpolated from donor-points to fringe-points. Each grid requires a zone of fringe-points at least three points deep, such that the seven point central difference stencil could be used without any special handling of points adjacent to the fringe-points. For the curvilinear grid, the fringe-points were simply the three outer points at each radial grid line (see Figure 1(b)). For the Cartesian grid, the fringe-points must be identified, typically during pre-processing, in order to include all grid points within a fixed area in the region covered by both the Cartesian and the cylindrical grid. This is set by an inner and outer radius defining the interpolation region, see red lines enclosing fringe-points on the Cartesian grid in Figure 1(c). Cartesian grid points that are closer to the solid than the inner radius of the fringe-point zone (or inside the solid), are hole-points. The hole-points are not used in the computations.

In the overset grid method implemented in the Pencil Code, there is no overlap between the two interpolation regions of Figures 1(b,c). That is, no fringe-points are used as donor-points. Hence, the interpolation is explicit, not implicit (Chesshire and Henshaw 1990). Note that if the bluff body enclosed by the body-fitted

grid were moving, the cost of inter-grid communication would be significantly increased due to the cost related to identifying new fringe and donor-points on the background grid at each new position of the bluff body.

At present, two types of interpolation are implemented for overset grid communication in the Pencil Code: bi-linear Lagrangian interpolation and bi-quadratic spline interpolation. Both methods have the advantage of avoiding oscillations in the interpolation interval, which is a common problem for high-order interpolation. The Lagrangian interpolation is a second-order accurate scheme, while the spline interpolation is third-order accurate. The illustration of donor-points and fringe-points in Figures 1(b,c) is for Lagrangian interpolation, where each fringe-point on one grid is interpolated from the 2×2 surrounding donor-points of the other grid. For spline interpolation, a zone of the 3×3 closest grid points are used as donor-points for interpolation of each fringe-point. Note that the interpolation is bi-linear or bi-quadratic in both two- and three-dimensions. This is due to the Cartesian and cylindrical grid having a shared z-axis ((x,y)-plane displayed in Figure 1), hence no interpolation is required in the z-direction.

At the solid–fluid interface, summation-by-parts finite-difference operators are used to enhance stability for time-dependent flow simulations (an unsteady wake develops for Re > 47). These operators are third-order accurate for the sixth-order centred finite-difference method. Details on these operators can be found in Strand (1994) (first derivatives) and Mattsson and Nordström (2004) (second derivatives).

The centred finite-difference schemes are non-dissipative, which can be detrimental due to the potential growth of high-frequency modes, leading to numerical instability. To some extent, the summation-by-parts boundary conditions suppress such instabilities, but these operators are not sufficient to suppress all oscillations in the solution on the curvilinear stretched grid. In particular, such oscillations are prominent in the density field. The detrimental effect of the high-frequency modes increases as the grid spacing decreases, which may lead to diverging solutions as the grid is refined.

To suppress the high-frequency modes, a high-order low-pass filter is used on the curvilinear part of the overset grid. The filter is a 10th order Padé filter, with boundary stencils of 8th and 6th order. On the interior of the domain, the filter is given by:

$$\alpha_f \hat{\phi}_{i-1} + \hat{\phi}_i + \alpha_f \hat{\phi}_{i+1} = \sum_{n=0}^{N} \frac{\alpha_n}{2}(\phi_{i+n} + \phi_{i-n}), \quad (5)$$

where $\hat{\phi}_k$ and ϕ_k are components k of the filtered and unfiltered solution vectors, respectively, α_f is a free parameter ($|\alpha_f| \leq 0.5$), $2N$ is the order of the filter, and α_n are fixed parameters dependent only on α_f (Visbal and Gaitonde 1999). Boundary stencils can be found in Gaitonde and Visbal (2000). The Padé filter is implicit, and requires the solution of a tri-diagonal linear system at grid points in the radial direction, and a cyclic tri-diagonal system at grid points in the direction tangential to the surface. The free parameter a_f was set to 0.1, for which filtering the solution once per Cartesian time step was found to be sufficient for a stable and accurate solution.

Note that the need for filtering to avoid numerical growth of high-frequency modes may be due to the use of a non-staggered grid, which is known to lead to weak pressure-velocity couplings (Ferziger and Peric 2002). Switching to a staggered grid, which has a stronger coupling between pressure and velocity, may reduce the need for filtering.

3. Performance

3.1. Assessment of accuracy

The spatial accuracy of the overset grid method was examined by simulating a steady flow past a circular cylinder at a Reynolds number of 20. A domain of size $L_x \times L_y = 10D \times 10D$ was used. The diameter of the curvilinear, body-fitted grid (henceforth called the cylinder grid) was three times the cylinder diameter.

An indicative measure of the accuracy of the method can be found by computing solutions on several grid refinement levels, and using the finest grid as the 'correct solution' when computing two-norm errors. The grids used in this accuracy assessment are listed in Table 1. An odd number of grid points was used in the directions that were not periodic, in order to have grid points that are aligned at each refinement level. A fixed (dimensionless) time step $\Delta t = 0.25 \times 10^{-3}$ was used for the Cartesian grid computations at all refinement levels. The small time step ensured that there was no violation of diffusive or advective time step restrictions on any of the grids. These restrictions are $\Delta \tau \leq C_v \Delta \chi_{\min}^2 / v$ and $\Delta \tau \leq$

Table 1. Grid refinement levels used in the assessment of accuracy of the overset grid method.

Refinement level	Cylinder grid $N_r \times N_\theta$	Cartesian grid $N_x \times N_y$
0	17×80	80×81
1	33×160	160×161
2	65×320	320×321
3	129×640	640×641

$C_u \Delta \chi_{\min}/(|\boldsymbol{u}| + c_s)$, respectively, where $\Delta \tau$ is the dimensional time step, $\Delta \chi_{\min}$ is the smallest grid spacing in any direction, and C_v and C_u are the diffusive and advective Courant numbers, respectively.

Hyperbolic sine functions were used for the stretching in the radial direction. The grid stretching parameters were set such that the ratio between the grid spacing normal and tangential to the surface was approximately one, both in the vicinity of the solid surface and in the interpolation region in the outer part of the cylinder grid. Furthermore, the number of grid points in the Cartesian and cylindrical grids were set in order to have similar grid spacings in the region of inter-grid interpolation. The resulting local time step on the cylindrical grid was $\Delta t_c = 0.2\Delta t$.

The main objective of the method, is to compute a very accurate boundary layer around the cylinder. This is crucial for the application to particle impaction simulations in Section 4 and in future studies. The L_2-error norms of flow variables are therefore considered along strips tangential to the cylinder surface as close as possible to the surface, in order to get an indication of the accuracy of the scheme in the boundary layer. Figure 2(a) depicts L_2-error norms of the density and the normal and tangential velocity components (with respect to the cylinder surface), computed with the two different interpolation methods. The norms were computed along a strip around the cylinder, at the grid point closest to the cylinder for the refinement level 0 (this corresponds to the 2nd point from the cylinder for refinement level 1, 4th for level 2, etc.). For certain applications (e.g. multiple-grid systems) the accuracy in the fringe-point zone can be of crucial importance. Therefore, equivalent L_2-error norms for the outermost grid point are included in Figure 2(b). Note that the computations with spline interpolation did not fully converge to a stable solution at the coarsest grid level, as indicated by the dashed lines between the first refinement results in Figure 2.

For both linear and spline interpolation, computation of the density was third-order accurate, the radial velocity component was between third- and fourth-order and the tangential velocity component was between second- and third-order accurate, at the grid point closest to the surface on the coarsest grid. The results suggest that the difference in accuracy between the interpolation methods is negligible in the immediate vicinity of the cylinder. At the outermost fringe-point the accuracy was somewhat lower than in the vicinity of the cylinder, with flow variables approximately second-order accurate regardless of interpolation method. For the density the order of accuracy was approximately half an order higher with spline interpolation than with linear interpolation, but negligible differences can be seen for velocity components.

For a more detailed picture of the formal order of accuracy of the overset grid method, consider Figure 3. This figure depicts the formal order of accuracy P, of the density and velocity components, computed along strips at increasing distance from the cylinder boundary (cylinder boundary at $r_c = 0.5$). The computations are based on the assumption that the L_2-error norm on a grid with grid spacing Δx can be expressed as $L_2(\Delta x) \sim \Delta x^p$, such that the order of accuracy P can be computed by:

$$P = \frac{\log(L_2(\Delta x)/L_2(\Delta x/2))}{\log 2}. \qquad (6)$$

In principle, the spline interpolation scheme is third-order accurate while the Lagrangian interpolation a second-order accurate method. The effect of using the different methods of interpolation can be seen in Figure 3. Some effect of the interpolation is seen, when considering the entire flow domain covered by the cylindrical grid. The difference is, however, much smaller than the theoretical difference in accuracy between the two interpolation schemes. The difference in order of accuracy of the radial velocity computations is 0.02–0.56, for which spline interpolation yielded the highest order (median $P = 2.49$ with spline interpolation, $P = 2.42$ with Lagrangian interpolation). A similar difference can be seen for the density. For the tangential velocity, on the other hand, there is no obvious best method. In the vicinity of the cylinder surface the difference between the Lagrangian and spline interpolation is negligible. Notice that the radial velocity component was computed with a very high-order of accuracy, $P \approx 5$ in this region. This is significantly more accurate than the more conservative suggestion of radial velocity accuracy between third-
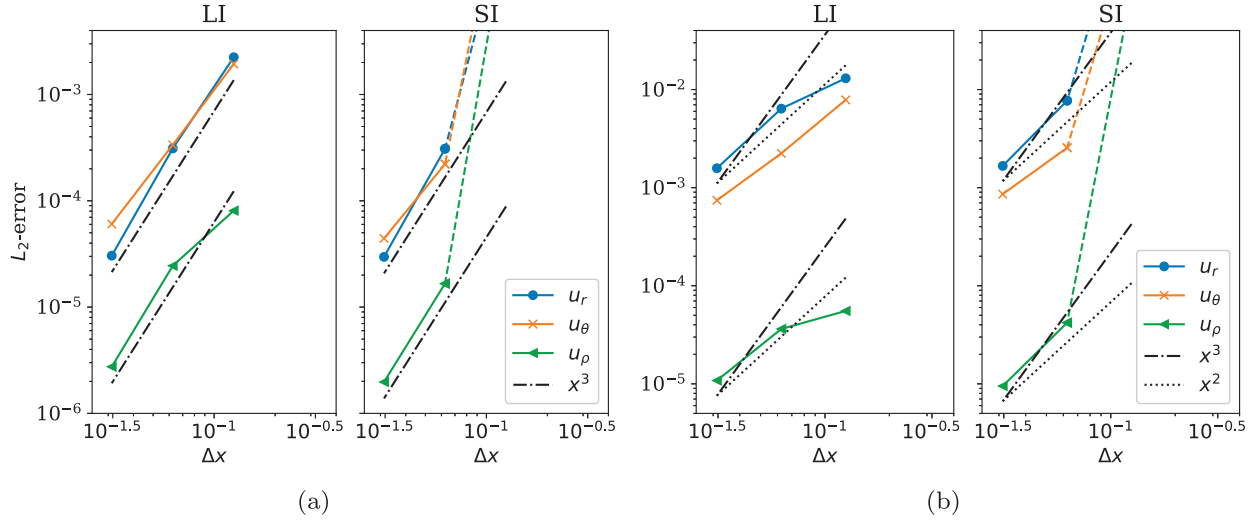
Figure 2. L_2-error norms of u_r, u_θ and ρ at varying refinement levels at the grid point (a) closest to the cylinder surface and (b) farthest away from the cylinder surface (for the coarsest grid). Results are for the computations with bi-linear Lagrangian interpolation (LI) and bi-quadratic spline interpolation (SI), with Δx (non-dimensional) grid spacing on the Cartesian grid.
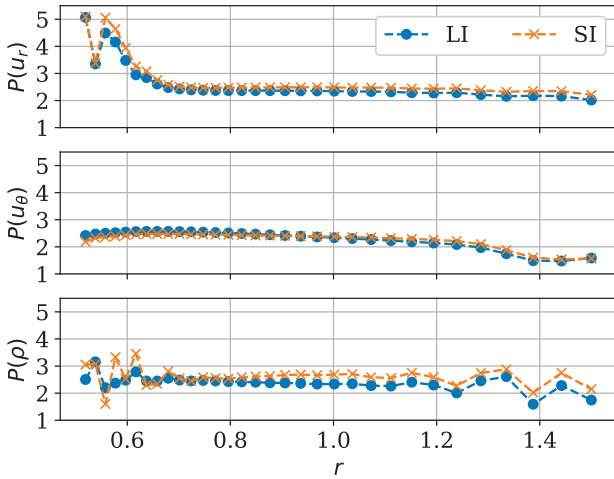

Figure 3. Formal order of accuracy of flow variables computed along strips tangential to the cylinder surface at non-dimensional radial position r, for upper refinement levels for flow with Re = 20 with Lagrangian interpolation (LI) and spline interpolation (SI).

and fourth-order, seen in Figure 2(a) (the results in Figure 2(a) correspond to the second point from the left in Figure 3).

The consideration of formal order of accuracy shows that the overset grid method is a high-order method ($P > 2$). No obvious distinction among the two interpolation schemes was found by this analysis, although the spline interpolation appeared to have a marginally higher accuracy for the density and radial velocity component.

3.2. Unsteady flow

The L_2-error norms are suggestive of the formal accuracy of the numerical method, but do not reveal the in use accuracy of the method for simulations in the unsteady flow regime. This must be determined, before arriving at a full-blown simulation of a particle-laden flow interacting with a cylinder in this flow regime.

A grid refinement study was performed for Re = 100, where unsteady vortex shedding developed in the cylinder wake. A domain with $L_x \times L_y = 10D \times 20D$ was used, with the cylinder in the centre of the domain. The resulting mean drag coefficient (C_D), root-mean-square lift coefficient (C_L') and Strouhal number (Str) were computed. The pressure and viscous forces on the cylinder were

$$\boldsymbol{F_p} = -\int p\big|_{r_c} \boldsymbol{dA} \approx -hr_c\Delta\theta \sum_{i=1}^{N_\theta} \hat{\boldsymbol{r}}_i p(r_c, \theta_i), \quad (7)$$

$$\boldsymbol{F_s} = \int \boldsymbol{\sigma}\big|_{r_c} dA \approx vhr_c\Delta\theta \sum_{i=1}^{N_\theta} \hat{\boldsymbol{\theta}}_i \rho(r_c, \theta_i) \frac{\partial u}{\partial r}\bigg|_{(r_c,\theta_i)}, \quad (8)$$

respectively, where h is the height of the cylinder and $\boldsymbol{\sigma}$ is the shear stress. With flow in the y-direction, the drag and lift forces, F_D and F_L, were found by taking the sum of the pressure and shear forces in y- and x-direction, respectively. These forces can be used to

calculate the drag and lift coefficients as follows:

$$C_D = \frac{F_D}{\frac{1}{2}\rho_0 U_0^2 A}, \qquad (9)$$

$$C_L = \frac{F_L}{\frac{1}{2}\rho_0 U_0^2 A}, \qquad (10)$$

where ρ_0 and U_0 are free-stream values of the density and velocity, respectively, and $A = 2hr_c$ is the projected frontal area of the cylinder. The Strouhal number is simply the vortex shedding frequency, non-dimensionalized by the free-stream velocity and cylinder diameter.

A grid refinement study of the unsteady flow was performed with both Lagrangian and spline interpolation on two differently sized overset grids. One had a cylindrical grid with diameter $3D$ (the same size that was used in the assessment of accuracy for the $Re = 20$), the other had diameter $5D$. Hence, there was a factor two difference in the radial length ($L_r = r_{cg} - r_c$, where r_{cg} is the outer cylinder grid radius) of the two cylindrical grids. At each refinement level, the smallest spacing in the radial direction was the same for the two different overset grids. The stretching properties were the same as that in the $Re = 20$ flow simulations (approximately quadratic cells in the vicinity of the surface and the interpolation region, and approximately equal grid spacing on the Cartesian and curvilinear grid in the interpolation region). Hence, the outer grid spacing on the larger cylindrical grid was larger than the outer grid spacing of the smaller cylindrical grid. Thus, a coarser Cartesian grid could be used for the overset grid with the larger cylinder grid. This, in turn, allowed for a larger time step on the background grid, but required more sub-cycles on the cylindrical grid for each Cartesian time step. Details on the grids used in this refinement study are listed in Table 2.

Results for the grid refinement at $Re = 100$ can be seen in Figure 4 and Table 3. In Figure 4, the dimensionless drag and lift coefficients, and the Strouhal number have been normalised by the result computed at the finest grid. Hence, the plots depict the relative deviation from the result at the 8th grid refinement level from Table 2. The values of the coefficients computed at this refinement level, for each of the four cases, are given in Table 3.

The dimensionless numbers converged quite rapidly for all of the tested cases. The best performance

Table 2. Grid refinement levels used in the grid refinement study for flow past a cylinder at $Re = 100$ with two differently sized cylindrical grids.

Refinement level	Δr_{min} $\times 10^2$	$r_{cg} = 3r_c$		$r_{cg} = 5r_c$	
		$N_r \times N_\theta$	$N_x \times N_y$	$N_r \times N_\theta$	$N_x \times N_y$
0	4.1	16×80	80×160	24×80	50×100
1	2.7	24×120	120×240	36×120	76×152
2	2.0	32×160	160×320	48×160	100×200
3	1.6	40×200	200×400	60×200	128×256
4	1.3	48×240	240×480	72×240	150×300
5	0.97	64×320	320×640	96×320	200×400
6	0.77	80×400	400×800	120×400	256×512
7	0.64	96×480	480×960	144×480	306×612
8	0.48	128×640	640×1280	192×640	408×816

Note: grid spacing Δr non-dimensionalized by the cylinder diameter.

Table 3. Mean drag coefficient (C_D), rms-lift coefficient (C_L') and strouhal number (Str) for $Re = 100$ computed at a domain $L_x \times L_y = 10D \times 20D$ with two different overset grids.

Coefficient	$r_{cg} = 3r_c$		$r_{cg} = 5r_c$	
	LI	SI	LI	SI
C_D	1.460	1.458	1.461	1.461
C_L'	0.2509	0.2450	0.2527	0.2522
Str	0.1763	0.1762	0.1763	0.1763

Notes: The resolution is given by the finest refinement levels in Table 2, and both lagrangian (LI) and spline interpolation (SI) cases are considered.

for grid independency was achieved with Lagrangian interpolation. Yet, even for the poorest result, the computation of the rms-lift coefficient at the smaller of the two cylindrical grids with spline interpolation, deviated less than 0.5% from the finest grid result, for grid refinement level ≥ 4. Some deviation is also seen in the lift coefficient of results computed on the large cylindrical grid with spline interpolation (less than 0.24% for refinement level ≥ 4). For the cases where Lagrangian interpolation was used for inter-grid communication, the deviation from results at refinement levels four to seven from the finest grid result is less than 0.15% for all coefficients (if only drag and Strouhal number are considered, the deviation is less than 0.064% for these cases). The difference between results obtained with quadratic spline and linear Lagrangian interpolation was particularly clear for the smaller cylinder grid. With a larger grid, it is not surprising that the effects from interpolation were reduced. Nevertheless, the best results on the larger grid were also achieved with Lagrangian interpolation.

For the steady flow simulations the spline interpolation yielded somewhat higher order of accuracy than the Lagrangian interpolation. The sub-par performance of spline interpolation for unsteady
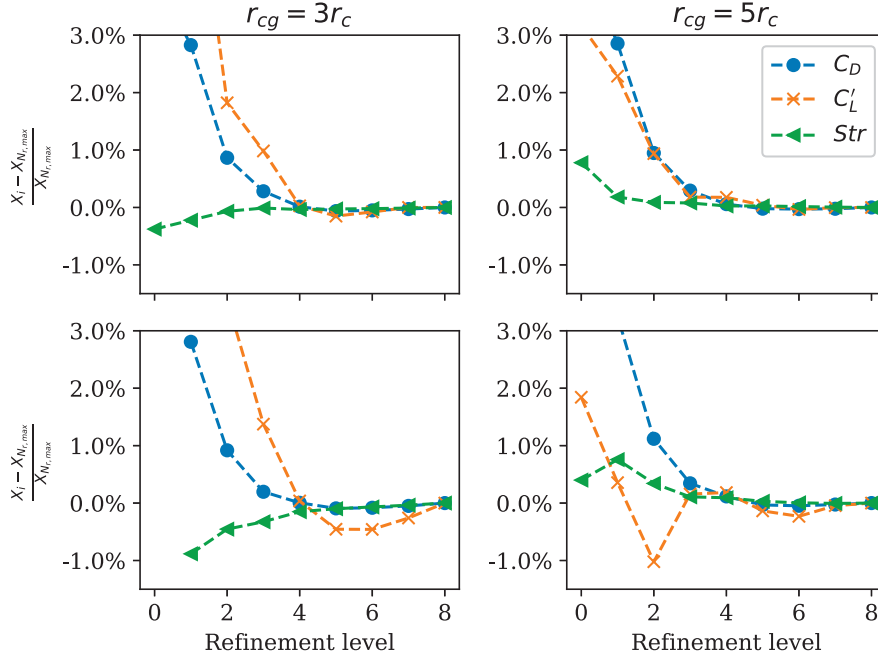
Figure 4. Normalized values for mean drag coefficient (C_D), rms-lift coefficient (C'_L) and Strouhal number (Str) for Re = 100 computed at different refinement levels (see Table 2) for overset grids with two sizes of radii for the body-fitted cylindrical grid, r_{cg}. Results are given for computations with Lagrangian interpolation (upper) and spline interpolation (lower).

simulations may be due to the overshoots for this non-linear interpolation, or perhaps, a larger mass loss during interpolation. No further speculation is conducted here, but it should be noted that the Lagrangian interpolation outperformed the spline interpolation for simulations of unsteady flow.

By considering the grid independent solutions in Table 3, used to normalise the grid refinement results, two particular factors can be noted. Firstly, by comparing the results for the two different interpolation schemes on the domain where the cylindrical grid has $r_{cg} = 5r_c$, it is evident that the computed drag, lift and Strouhal number were independent of the inter-grid communication. This is in contrast to the $r_{cg} = 3r_c$ results, but in accordance with an intuitive understanding of the problem: the farther away from the cylinder boundary the interpolation is performed, the less it affects computation of quantities at the boundary. Note, however, that even though the drag and lift forces were computed at the surface boundary, these coefficients also depend on the flow upstream and downstream of the cylinder. The results therefore suggest that the flow surrounding the cylinder was negligibly impacted by the interpolation method selected when the larger r_{cg} was used for the cylinder grid.

By comparing the results for C_D and C'_L on the differently sized cylinder grids, computed with Lagrangian interpolation, the dependency on cylinder grid size was found to be small. There was a small difference in the computed lift coefficient (somewhat higher for the larger cylinder grid). Although the results are grid independent, neither of the values are quantitatively accurate for the drag or lift of a cylinder in a cross flow at Re = 100. The small difference in computed lift may be due to blockage effects.

To confirm that the grid independent solutions yielded accurate flow predictions a simulation was also conducted on a large domain, $L_x \times L_y = 50D \times 50D$, for the two different grid sizes used above. Since Lagrangian interpolation had the best performance for the unsteady flow simulations, only this interpolation procedure was used. The grid spacing corresponding to grid refinement level five in Table 2 was used on the large square domain. The computed flow quantities showed good agreement with previous studies performed on similar domain sizes (see Table 4). Note that for the simulations on a large square domain there was a negligible difference between the results from the different overset grid simulations. Using a larger cylinder grid will reduce the total number of grid points in

Table 4. Comparison with previous studies.

	C_D	C'_L	St
Li et al. (2009)	1.336	–	0.164
Pan (2006)	1.32	0.23[*]	0.16
Posdziech and Grundmann (2007)	1.350	0.234[*]	0.167
Qu et al. (2013)	1.326	0.219	0.166
Present, $r_{cg} = 3r_c$	1.346	0.235	0.166
Present, $r_{cg} = 5r_c$	1.346	0.234	0.166

Notes: The studies were performed on domains with streamwise length $60 \leq L_x/D \leq 100$ and spanwise length $40 \leq L_x/D \leq 100$. The present study used $L_x = L_y = 50D$. Results from the present study are for domains covered by two differently sized overset grids, with inter-grid interpolation performed by bi-linear lagrangian interpolation. The asterisk on some values of C'_L denotes where only the amplitude of the lift was given. The asterisk mark a lift amplitude scaled by $1/\sqrt{2}$ to get the root-mean-square lift coefficient, a valid scaling for the sinusoidal-like lift coefficient (with mean value zero).

the simulations, which is a major advantage on large domains.

4. Particle deposition on a circular cylinder in a laminar cross flow

Direct numerical simulations with a large number of particles suspended in the flow have been performed to assess the performance of overset grids on a more complex and demanding simulation than the simple flow past a cylinder at low Reynolds numbers.

The particle deposition simulations are based on the study by Haugen and Kragset (2010), where particle-laden flow simulations were performed over a range of Reynolds numbers on a moderately sized flow domain ($6D \times 12D$). The analysis is not repeated here, but a brief introduction to the method used for particle representation and deposition is included. The particle-laden flow simulations were performed on a domain exactly the same size as in Haugen and Kragset (2010), with Reynolds number 100.

4.1. Particle equations

The particles are tracked using a Lagrangian formalism, where the particle velocity and position are described by:

$$\frac{d\boldsymbol{v}_p}{dt} = \frac{\boldsymbol{F}_{D,p}}{m_p}, \tag{11}$$

$$\frac{d\boldsymbol{x}_p}{dt} = \boldsymbol{v}_p, \tag{12}$$

where $\boldsymbol{v}_p$, $\boldsymbol{x}_p$ and m_p are the velocity, centre of mass position and mass of the particle, respectively. The force $\boldsymbol{F}_{D,p}$ acting upon a spherical particle is the drag force:

$$\boldsymbol{F}_{D,p} = \frac{1}{2C_c}\rho C_{D,p}A_p |\boldsymbol{u} - \boldsymbol{v}_p| (\boldsymbol{u} - \boldsymbol{v}_p), \tag{13}$$

where $A_p = \pi d_p^2/4$ is the cross sectional area of the particle and

$$C_c = 1 + \frac{2\lambda}{d_p}\left(1.257 + 0.4e^{(-1.1d_p/2\lambda)}\right), \tag{14}$$

is the Stokes–Cunningham factor (with parameters set for air) for a particle with diameter d_p. The mean free path λ accounts for the fact that for very small particles, the surrounding medium can no longer be regarded as a continuum but rather as discrete particles. The particle drag coefficient is given by:

$$C_{D,p} = \frac{24}{\text{Re}_p}\left(1 + 0.15\text{Re}_p^{0.687}\right), \tag{15}$$

for particle Reynolds number $\text{Re}_p = d_p|\boldsymbol{v}_p - \boldsymbol{u}|/\nu \lesssim 1000$. With this, the particle drag force can be rewritten as

$$\boldsymbol{F}_{D,p} = \frac{m_p}{\tau_p}(\boldsymbol{u} - \boldsymbol{v}_p), \tag{16}$$

where

$$\tau_p = \frac{Sd_p^2 C_c}{18\nu(1 + f_c)} \tag{17}$$

is the particle response time, with $f_c = 0.15\text{Re}_p^{0.687}$ and $S = \rho_p/\rho$. Note that this becomes Stokes drag in the limit $C_c = 1$ and $f_c = 0$. Using the convention of Haugen and Kragset (2010), the Stokes number ($St = \tau_p/\tau_f$) is defined with a fluid time scale:

$$\tau_f = \frac{D}{2U_0}. \tag{18}$$

The fluid velocity was interpolated from surrounding grid points by bi-linear interpolation on the Cartesian grid and bi-quadratic interpolation on the curvilinear grid. The order of the interpolation is higher on the curvilinear grid as the velocity components (the radial, in particular) are close to quadratic near the cylinder surface. For three-dimensional simulations, linear interpolation is used for the velocity component along the z-direction (the cylinder's spanwise direction) on all grids.

For particles very close to the cylinder surface, special handling was used to interpolate the radial component of the fluid velocity. Very close to the cylinder refers to within one grid point from the surface,

or alternatively, within the pre-calculated momentum thickness of the boundary layer. The special handling in use for particles at such positions was a quadratic interpolation that guarantees no overshoots. Since all velocities are zero at the surface, this was achieved by:

$$u_{r,p} = u_{r,g} \left(\delta r_p / \delta r_g \right)^2, \qquad (19)$$

where $u_{r,p}$ and $u_{r,g}$ are the radial velocity component at the position of the particle and at the position of the interception between a surface normal and the first grid line away from the surface, respectively. The distances δr_p and δr_g are from the cylinder surface to the particle's centre of mass and to said grid line, respectively.

4.2. Particle impaction

After the flow developed into periodic vortex shedding, particles were inserted continuously at the inlet. The particles were inserted randomly, as a homogeneous distribution over a rectangular cross-section encompassing particle trajectories that could impact the cylinder. From here the particles were convected downstream, and removed from the flow either by impacting the cylinder or by reaching the outlet (see Figure 5). An impaction was registered (and the particle removed) if the distance between the cylinder surface and the particle's centre of mass was less than

or equal to $d_p/2$. Every particle impaction simulation was run until all particles were removed from the flow. In total 1.1×10^7 particles were inserted, with Stokes numbers of 0.01–10 in a progressive particle distribution with respect to particle radius.

The impaction efficiency ($\eta = N_{imp}/N_{ins}$) can be split into front- (η_f) and back-side (η_b) impaction. At the low Reynolds number flow in this study, back-side impaction rarely occurred so only front-side impaction was in focus. Figure 6 depicts the particle front-side impaction, compared to literature results. The results were computed with grid spacing defined as refinement level four in Table 2, for the $r_{cg} = 3r_c$ case with Lagrangian interpolation. With the $L_x \times L_y = 6D \times 12D$ domain a grid with $(N_r \times N_\theta) + (N_x \times N_y) = (48 \times 240) + (144 \times 288)$ points was used. The results from Haugen and Kragset (2010) were computed on an equidistant grid with 512×1024 grid points, using an immersed boundary method to resolve the cylinder surface.

The particle impaction results from this study agree very well with the results from the literature, even though the results of the present study were computed on a grid with only 10.1% as many grid points as used by Haugen and Kragset (2010). An additional efficiency improvement was achieved, due to the use of a time step that was 3.5 times larger. This was possible because of the time step's proportionality to the grid
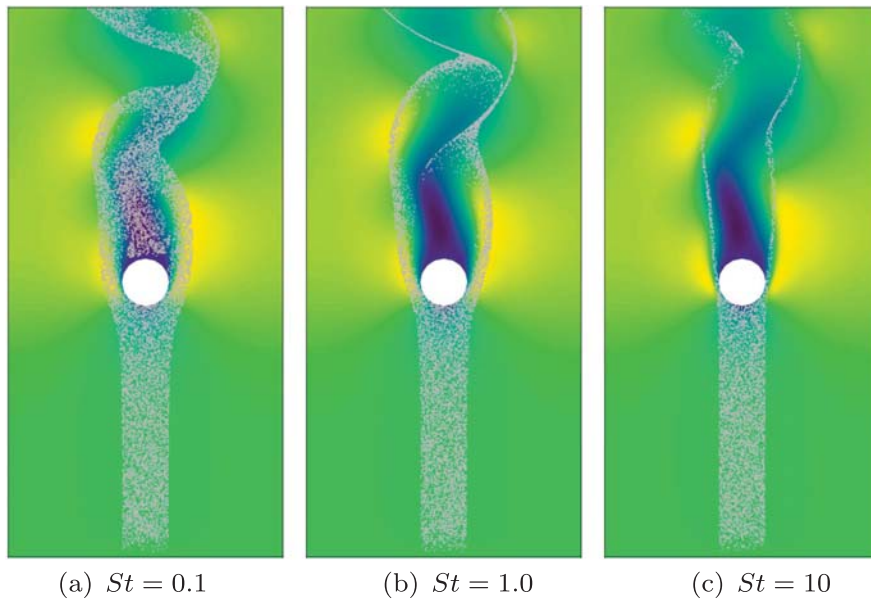

(a) $St = 0.1$ (b) $St = 1.0$ (c) $St = 10$

Figure 5. Particle-laden flow interacting with a circular cylinder at Re = 100. An unhindered particle will cross the flow domain, from the inlet (bottom) to the outlet (top) in approximately two shedding periods at this Reynolds number. Contours of the streamwise velocity component make up the background. (a) $St = 0.1$ (b) $St = 1.0$ (c) $St = 10$.
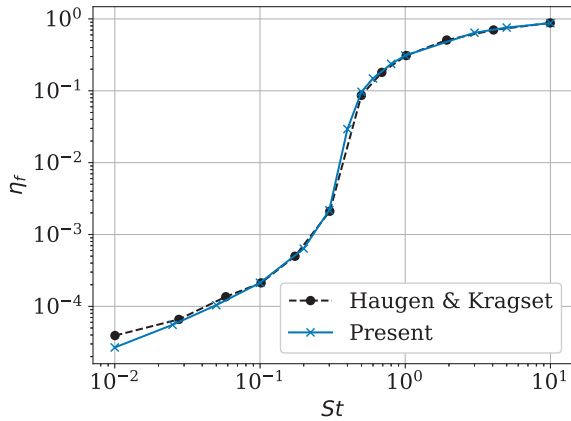
Figure 6. Front-side impaction efficiency (η_f) as a function of Stokes number (*St*) for Reynolds number 100. Present results compared to a previous study by Haugen and Kragset (2010).

spacing and the local time step restrictions, though some extra work was necessary at each time step (computation on two grids, communication of data, filtering on cylinder grid, etc.). Note that for very small particles, the time step can also be restricted by the particle time scale, that is, the time step must be small enough to resolve the time-dependent particle equations. Particles are updated only at the Cartesian time step.

4.3. Investigating the accuracy of the computed impaction efficiencies

The coarseness of the grid used in the computation of particle impaction efficiencies allow for the assessment of the assumptions that must be made in order to regard these impaction results as quantitatively accurate. The assumptions are, firstly, that blockage effects from the limited domain (with $L_x \times L_y = 6D \times 12D$) have a negligible impact on the particle impaction. Secondly, it was assumed that the coarsest resolution where grid independency of drag and lift coefficients was reached was sufficiently fine for the particle simulations, i.e. that the transport of the particles was dependent on an accurate flow field only.

A critical assessment of these assumptions led to the expectation of higher impaction for particles on a domain where the blockage effect is large, due to a squeezing of the flow field and, consequently, less particles being directed away from the cylinder. In particular, this is expected to affect particles that follow the flow to a large extent, i.e. particles with small Stokes numbers. Further, the flow velocities at particle

positions are not only dependent on an accurately computed flow field, but also on accurate interpolation. The latter aspect can be very sensitive to grid spacing, even if the flow is resolved accurately. Haugen and Kragset (2010) used linear interpolation to compute flow velocity at particle positions, except within the grid point closest to the surface, where an expression similar to that of Equation (19) was used. Linear interpolation of velocities that are proportional to $(\delta r)^2$ (as the upstream flow field at the centre-line through the cylinder is) will lead to a systematic over-estimation. Hence, an over-prediction in particle impaction can be expected from their results. What is important to determine in this respect, is how large this possible over-prediction is, and for what particle sizes it occurs.

To investigate the accuracy of the computed impaction efficiencies particle-laden flow simulations were conducted at a larger domain size, $L_x \times L_y = 10D \times 20D$, as used in the grid independence study of Section 3.2. For this larger domain several refined grids were used. These utilised refinement levels 4–7 in Table 2, with $r_{cg} = 3r_c$. Thus, from 48 (coarsest) to 96 (finest) grid points were used in the radial direction on the cylindrical grid, and the background grid was refined accordingly. The number of inserted particles was 1.1×10^7, where 7×10^6 were particles with $St \leq 0.1$. The results are seen in Figure 7.

Very few of the smallest particles deposit on the cylinder. To get sufficient particle impactions at the smallest Stokes numbers for reliable statistics, particles with $St \leq 0.1$ were only inserted over a region covering one tenth of the cylinder's projected area, at its centreline. The inserted particle count was scaled correspondingly (multiplied by 10) during post-processing. No small Stokes number particles inserted outside the insertion area would be expected to hit the cylinder. To confirm this, a simulation was conducted with particles with $St = 0.05$ and 0.1, inserted over the whole projected cylinder area. The results are included as black circles (o) in Figure 7. The difference in impaction efficiency among particles inserted by the two different methods was negligible.

From Figure 7 it is clear that the blockage effect from the limited domain size had a significant effect on the particle impaction efficiencies. For $St \leq 0.5$ this effect was larger than 10%, and increased as the Stokes number decreased. The largest difference in impaction efficiencies was seen at $St = 0.01$, where
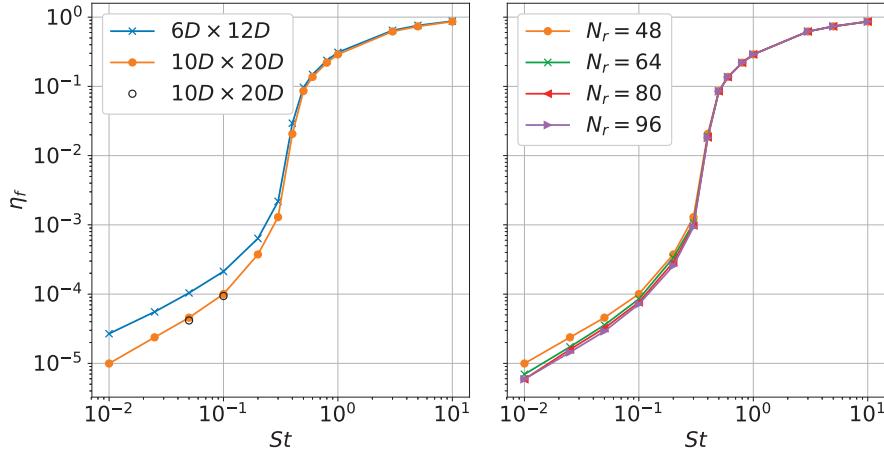
Figure 7. Front-side impaction efficiency (η_f) as a function of Stokes number (St) for Reynolds number 100 for different domain sizes (left) and grid resolutions (right).

2.7 times more impactions occurred for the smallest domain size. The resolution played a smaller, but not insignificant, role in the impaction efficiencies. Increasing from the coarsest grid, with $N_r = 48$, to $N_r = 64$, noticeably reduced the impaction efficiencies. The reduction was more than 10% for $St \leq 0.3$. A further refinement of the grid had only a small effect (negligible for $N_r \geq 80$). Comparing the results from the larger domain with $N_r = 80$ to those by Haugen and Kragset (2010) suggests that Haugen & Kragset found a qualitatively correct result, but have somewhat quantitatively over-predicted the particle impaction, in particular in the boundary interception region (where $St \lesssim 0.3$). For the smallest Stokes number ($St = 0.01$) the over-prediction is of approximately a factor 6.3. At $St = 0.1$ this factor is 2.8. The previously published results agree with the new results for $St \geq 0.5$.

5. Concluding remarks

In this work, a high-order overset grid method has been presented. The method uses high-order finite-difference discretization to solve the compressible Navier–Stokes equations on several grids, and communicates necessary flow data between the grids by linear or quadratic interpolation. Unique to the overset grid implementation described here, is the use of local time step restriction and summation-by-parts finite-difference operators. The relaxed time stepping restriction on the coarser grid is very efficient for a weakly compressible flow, while the summation-by-parts operators enhance numerical stability together

with the use of Padé filtering. The purpose of developing the method was to compute particle impaction on a cylinder in a cross flow, and for this purpose a body-fitted cylindrical grid is an appropriate choice to resolve the boundary layer around the cylinder with high accuracy.

An investigation of the formal order of accuracy of the overset grid implementation revealed that high-order accuracy was indeed reached. Flow variables where computed with median order $P \approx 2.5$, regardless of the use of bi-linear interpolation or bi-quadratic interpolation for communication. Near the surface, the radial velocity component reached an accuracy of fifth-order. For unsteady flow, the method converged rapidly to grid independent solutions for the essential flow variables (drag, lift and Strouhal number). For these computations, using bi-linear interpolation was beneficial, yielding the most rapid convergence to grid independent solutions as the grid was refined. Using a larger cylindrical grid, with a radius five times as large as the cylinder radius, decreased the effect of the inter-grid interpolation.

When applied to the problem of inertial particles impacting on a cylinder, impaction efficiencies of previously published results were reproduced at a significantly reduced computational cost. A coarser background grid was utilised to resolve the flow, which yielded both a much smaller number of grid points (90% reduction in 2D) and the possibility of using a larger time step.

A critical assessment of the particle impaction results revealed that the limited domain size had a significant impact on impaction, particularly for the

smaller Stokes numbers. Further, although the flow was deemed grid independent, using a finer grid, and thus a more accurate interpolation of flow velocity, reduced the number of particles that hit the cylinder. The resulting impaction curves suggested that particle impaction has been over-estimated in the previous studies, in particular for very small particles where impaction occurs by boundary interception.

The overset grid method implementation in the Pencil Code is now ready for three-dimensional simulations, and DNS studies of particle impactions on a cylinder with Reynolds number for real-world application (a factor 10–20 larger than the investigation here, for industrial boilers) is within reach. However, even with the highly accurate and efficient method presented here, increasing the Reynolds number and computing three-dimensional flow will be computationally costly. The magnitude of the Reynolds numbers that can be considered will largely depend on the Stokes numbers of the particles, and the acceptable accuracy when particle impaction efficiencies are computed. If the focus is not just qualitative trends, but quantitatively accurate results, a careful assessment of grid independence is recommended (not just for flow variables, but for the particle impaction itself), and great care is required when selecting the domain size and setting up the simulations.

ORCID

Jørgen R. Aarnes 🆔 http://orcid.org/0000-0002-5899-2597

References

Aarnes, J. R., N. E. L. Haugen, and H. I. Andersson. 2019. "Inertial Particle Impaction on a Cylinder in Turbulent Cross-Flow At Modest Reynolds Numbers." *International Journal of Multiphase Flow* 111: 53–61.

Beckmann, A. M., M. Mancini, R. Weber, S. Seebold, and M. Müller. 2016. "Measurements and CFD Modeling of a Pulverized Coal Flame with Emphasis on Ash Deposition." *Fuel* 167: 168–179.

Benek, J. A., P. G. Buningt, and J. L. Steger. 1985. "A 3-D Chimera Grid Embedding Technique." In *AIAA 7th Computational Fluid Dynamics Conference*, AIAA Paper No. 1523.

Brandenburg, A., and W. Dobler. 2002. "Hydromagnetic Turbulence in Computer Simulations." *Computer Physics Communications* 147 (1–2): 471–475.

Chesshire, G., and W. D. Henshaw. 1990. "Composite Overlapping Meshes for the Solution of Partial Differential Equations." *Journal of Computational Physics* 90 (1): 1–64.

Chicheportiche, J., and X. Gloerfelt. 2012. "Study of Interpolation Methods for High-Accuracy Computations on Overlapping Grids." *Computers and Fluids* 68: 112–133.

Ferziger, J. H., and M. Peric. 2002. *Computational Methods for Fluid Dynamics*. 3rd ed. Berlin: Springer-Verlag.

Gaitonde D. V., and M. R. Visbal. 2000. "Padé-Type Higher-Order Boundary Filters for the Navier-Stokes Equations." *AIAA Journal* 38 (11): 2103–2112.

García Pérez, M., E. Vakkilainen, and T. Hyppänen. 2016. "Unsteady CFD Analysis of Kraft Recovery Boiler Fly-Ash Trajectories, Sticking Efficiencies and Deposition Rates with a Mechanistic Particle Rebound-Stick Model." *Fuel* 181: 408–420.

Haugen, N. E. L., and S. Kragset. 2010. "Particle Impaction on a Cylinder in a Crossflow As Function of Stokes and Reynolds Numbers." *Journal of Fluid Mechanics* 661: 239–261.

Haugen, N. E. L., S. Kragset, M. Bugge, R. Warnecke, and M. Weghaus. 2013. "MSWI Super Heater Tube Bundle: Particle Impaction Efficiency and Size Distribution." *Fuel Processing Technology* 106: 416–422.

Israel, R., and D. E. Rosner. 1982. "Use of a Generalized Stokes Number to Determine the Aerodynamic Capture Efficiency of Non-Stokesian Particles From a Compressible Gas Flow." *Aerosol Science and Technology* 2 (1): 45–51.

Li, Y., R. Zhang, R. Shock, and H. Chen. 2009. "Prediction of Vortex Shedding from a Circular Cylinder Using a Volumetric Lattice-Boltzmann Boundary Approach." *European Physical Journal: Special Topics* 171 (1): 91–97.

Mattsson, K., and J. Nordström. 2004. "Summation by Parts Operators for Finite Difference Approximations of Second Derivatives." *Journal of Computational Physics* 199 (2): 503–540.

Mavriplis, D. J. 1997. "Unstructured Grid Techniques." *Annual Review of Fluid Mechanics* 29 (1): 473–514.

Meakin, R. L. 1995. "The Chimera Method of Simulations for Unsteady Three-Dimensional Viscous Flow." In *Computational Fluid Dynamics Review*, edited by M. Hafez and K. Oshima, 70–86. New York, NY: Wiley.

Mittal, R., and G. Iaccarino. 2005. "Immersed Boundary Methods." *Annual Review of Fluid Mechanics* 37 (1): 239–261.

Owen, S. J. 1998. "A Survey of Unstructured Mesh Generation Technology." In *Proceedings of 7th International Meshing Roundtable*, Dearborn, MI, 239–267. Sandia National Laboratories.

Pan, D. 2006. "An Immersed Boundary Method on Unstructured Cartesian Meshes for Incompressible Flows with Heat Transfer." *Numerical Heat Transfer, Part B: Fundamentals* 49 (3): 277–297.

Pärt-Enander, E., and B. Sjögreen. 1994. "Conservative and Non-Conservative Interpolation Between Overlapping Grids for Finite Volume Solutions of Hyperbolic Problems." *Computers and Fluids* 23 (3): 551–574.

Peskin, C. S. 1972. "Flow Patterns Around Heart Valves: A Numerical Method." *Journal of Computational Physics* 10 (2): 252–271.

Poinsot, T. J., and S. K. Lele. 1992. "Boundary Conditions for Direct Simulations of Compressible Viscous Flows." *Journal of Computational Physics* 101 (1): 104–129.

Posdziech, O., and R. Grundmann. 2007. "A Systematic Approach to the Numerical Calculation of Fundamental Quantities of the Two-Dimensional Flow Over a Circular Cylinder." *Journal of Fluids and Structures* 23 (3): 479–499.

Qu, L., C. Norberg, L. Davidson, S.-H. Peng, and F. Wang. 2013. "Quantitative Numerical Analysis of Flow Past a Circular Cylinder At Reynolds Number Between 50 and 200." *Journal of Fluids and Structures* 39: 347–370.

Sherer, S. E., and J. N. Scott. 2005. "High-Order Compact Finite-Difference Methods on General Overset Grids." *Journal of Computational Physics* 210 (2): 459–496.

Steger, J. L., and J. A. Benek. 1987. "On the Use of Composite Grid Schemes in Computational Aerodynamics." *Computer Methods in Applied Mechanics and Engineering* 64 (1–3): 301–320.

Steger, J. L., F. C. Dougherty, and J. A. Benek. 1983. "A Chimera Grid Scheme." In *Advances in Grid Generation*, edited by K.N. Ghia and U. Ghia, 59–69. ASME FED-5.

Strand, B. 1994. "Summation by Parts for Finite Difference Approximations for D/dx." *Journal of Computational Physics* 110 (1): 47–67.

Tannehill, J. C., D. Anderson, and R. H. Pletcher. 1997. *Computational Fluid Mechanics and Heat Transfer*. 2nd ed. Philadelphia, PA: Taylor and Francis.

The Pencil Code. 2018. (pencil-code.nordita.org [Internet]). Stockholm (SE): NORDITA; [updated 2018 May 01]. https://github.com/pencil-code.

Versteeg, H. K., and W. Malalasekera. 2007. *An Introduction to Computational Fluid Dynamics: The Finite Volume Method*. 2nd ed. Harlow: Pearson Education.

Visbal, M. R., and D. V. Gaitonde. 1999. "High-Order-Accurate Methods for Complex Unsteady Subsonic Flows." *AIAA Journal* 37 (10): 1231–1239.

Völkner, S., J. Brunswig, and T. Rung. 2017. "Analysis of Non-Conservative Interpolation Techniques in Overset Grid Finite-Volume Methods." *Computers and Fluids* 148: 39–55.

Vreman, A. W. 2016. "Particle-Resolved Direct Numerical Simulation of Homogeneous Isotropic Turbulence Modified by Small Fixed Spheres." *Journal of Fluid Mechanics* 796: 40–85.

Vreman, A. W., and J. G. M. Kuerten. 2018. "Turbulent Channel Flow Past a Moving Array of Spheres." *Journal of Fluid Mechanics* 856: 580–632.

Williamson, J. H. 1980. "Low-Storage Runge-Kutta Schemes." *Journal of Computational Physics* 35 (1): 48–56.

Yoo, C. S., Y. Wang, A. Trouvé, and H. G. Im. 2005. "Characteristic Boundary Conditions for Direct Simulations of Turbulent Counterflow Flames." *Combustion Theory and Modelling* 9 (4): 617–646.

Zang, Y., and R. L. Street. 1995. "A Composite Multigrid Method for Calculating Unsteady Incompressible Flows in Geometrically Complex Domains." *International Journal for Numerical Methods in Fluids* 20 (5): 341–361.